Supporting Information

An Effective Descriptor for the Screen of Electrolyte Additives for the Stabilization of Zn Metal Anodes

Lin Hong[a], Jingzhuo Guan[a], Yiwei Tan[a], Yao Chen[a], Yu-Si Liu[b], Wei Huang*[a], Chunyang Yu[a], Yongfeng Zhou[a], Jie-Sheng Chen[a], and Kai-Xue Wang*[a]

[a]School of Chemistry and Chemical Engineering, State Key Laboratory of Metal Matrix Composites, Shanghai Jiao Tong University, 800 Dongchuan Road, Shanghai 200240, P. R. China.

E-mail: hw66@sjtu.edu.cn (W. Huang); k.wang@sjtu.edu.cn (K. X. Wang)

[b]College of Smart Energy, Shanghai Jiao Tong University, 800 Dongchuan Road, Shanghai 200240, P. R. China.

Experimental Section

Preparation of Electrolyte: $ZnSO_4 \cdot 7H_2O$ (Macklin, 99%) was dissolved into deionized water to prepare 2.0 M $ZnSO_4$ electrolyte. The electrolytes with different weight ratios of pectin (0.05, 0.1, 0.15, and 0.2 wt%) were prepared by adding a certain amount of pectin powder (Shanghai yuanye Bio-Technology Co., Ltd) into the $ZnSO_4$ electrolytes and stirring for 24 h. The obtained $ZnSO_4$/pectin mixed electrolytes were stored in the refrigerator. The optimized weight ratio of pectin was 0.1 wt%, and the optimal electrolyte was denoted as pectin additive.The electrolyte with

other anionic polysaccharide was prepared by replacing the pectin additive by carrageenan or hyaluronic acid with a weight ratio of 0.1 wt%. The electrolyte with organic solvent (Adamas-beta) was prepared by adding DMSO, DMF, NMF, or DX into aqueous 2.0 M $ZnSO_4$ with a volume ratio of 10 vol%, respectively.

Preparation of MnO_2: In a typical process, 2.0 mL H_2SO_4 solution (0.5 M) was added into 90 mL $MnSO_4$ solution (3.0 mM). After continuously stirring for 10 min, 20 mL $KMnO_4$ solution (0.1 M) was added into the above solution drop by drop and stirred for 2 h. The above mixture was transferred into a Teflon-lined autoclave and maintained at 120 °C for 12 h. After cooling to room temperature, the product was collected by centrifugation, washed thoroughly with deionized water, and dried at 60 °C in a vacuum oven for 12 h.

Materials characterizations: The deposition morphologies were observed on confocal laser scanning microscope (CLSM, Keyence VKX3000). X-ray diffraction (XRD) patterns were characterized by a Rigaku Mini Flex 600 diffractometer using Cu Kα-radiation (λ= 1.5418 Å). The surface morphologies of the cycled anodes were performed on field emission scanning electron microscope (SEM, RISE-MAGNA). The *in situ* optical visualization observation of Zn plating/stripping behavior was collected by an optical microscope (LEICA DM 4000).

Electrochemical measurements: The Zn||Zn, Zn||Cu, and Zn||MnO_2 cells were assembled by CR2032-type cells and measured on a Neware battery test system (CT-4008T-5V20mA-164, Shenzhen, China) under galvanostatic charge/discharge condition. The long-term cycling stability

of Zn anode was carried out on Zn symmetrical cells with pure $ZnSO_4$ electrolyte or $ZnSO_4$-pectin electrolyte. Coulombic efficiency (CE) measurements that reflect the reversibility of anode were performed on asymmetrical Zn||Cu cells. The Zn||MnO_2 full cells were assembled with Zn anode, MnO_2 cathode, glass fiber separators, and aqueous electrolyte. Cyclic voltammetry (CV), linear sweep voltammetry (LSV), corrosion test, and electrochemical impedance spectroscopy (EIS) were measured on an electrochemical workstation (CHI760E, China).

The depth of discharge (DOD) was calculated as follows,

$$DOD_{(\%)} = \frac{C_{actual}}{C_{theoretical}} \times 100\% = \frac{I \times t \times S}{m \times C_{theoretical}} \times 100\%$$

Where C_{actual} (mAh g^{-1}) is actual specific capacity of deposited/stripped Zn, $C_{theoretical}$ (mAh g^{-1}) is theoretical specific capacity of Zn anode (~820 mAh g^{-1}), I (mA cm^{-2}) is the current density during plating/stripping process, t (h) is the deposited/stripped time of Zn, S (cm^2) and m (g) are actual area and mass of electrode, respectively.

Computational Method: Density functional theory (DFT) calculations were carried out using projector-augmented wave (PAW) method as implemented in Vienna ab initio simulation package (VASP). A generalized gradient approximation (GGA) of Perdew-Burke-Ernzerhof (PBE) functional was employed to describe the exchange-correlation interaction. An energy cutoff of 450 eV and Gamma centered 2×2×1 k-points mesh were applied to all calculations. The structures were relaxed until the forces and total energy on all atoms were converged to less than -0.05 eV $Å^{-1}$ and 1×10^{-5} eV, respectively. To evaluate the interaction between Zn matrix and pectin, the binding energy (E_b) was calculated as follows,

$$E_b = E_{Total} - E_{Zn} - E_{pectin}$$

where E_{pectin} is the energy of pectin compound. E_{Total} is the total energy of pectin compound adsorbed on Zn matrix. E_{Zn} is the energy of Zn matrix. The lower the binding energy, the stronger the interaction between Zn matrix and pectin. The dissociation energy barriers of H_2O on the surface are calculated using the climbing-image nudged elastic band (CI-NEB) method.

To evaluate the desolvation process, the binding energy between H_2O and pectin was calculated as follows,

$$E_b = E_{Total} - E_{H2O} - E_{pectin}$$

where E_{pectin} and E_{Total} are the total energy of compound before and after H_2O adsorption, respectively. E_{H2O} is the energy of a single H_2O molecule. The electrostatic potential (ESP) analyses and HOMO-LUMO analyses are based on the B3LYP/6-31G (d, p) of Gaussian 09w software package.

Electric field simulation: In order to simulate the dynamic evolution of Zn deposition on electrodes in different electrolytes, a Finite Element Analysis (FEA) model was performed using COMSOL Multiphysics 6.1 software with the “Phase Field” module. The size of the entire two-dimensional model for order parameter distribution analysis was set to 6.0×6.0 μm. A transient simulation of the process was carried out in an area filled with electrolyte.

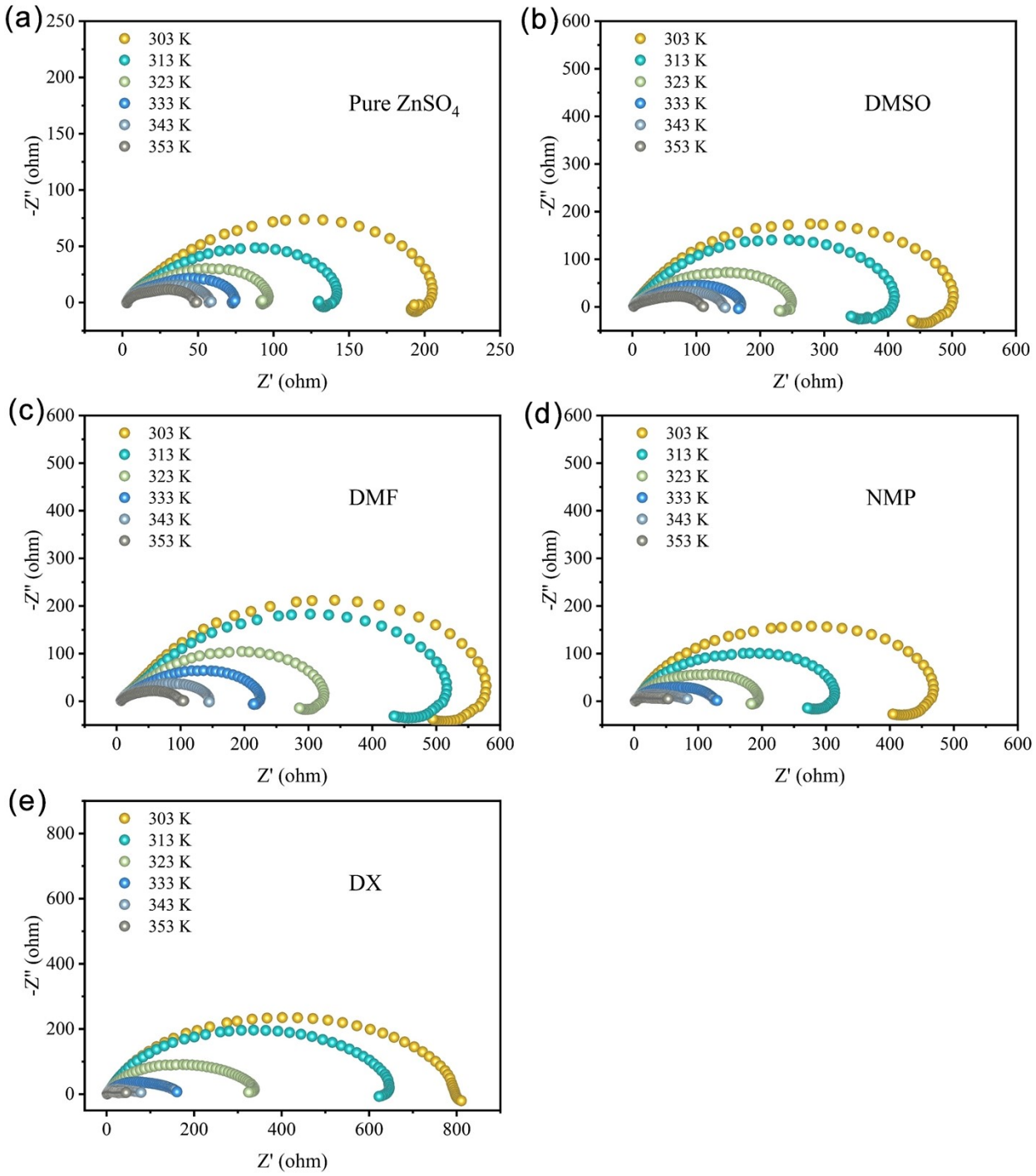

Figure S1 Nyquist plots of symmetric cells with (a) pure $ZnSO_4$, (b) DMSO, (c) DMF, (d) NMP, and (e) DX additive at different temperatures.

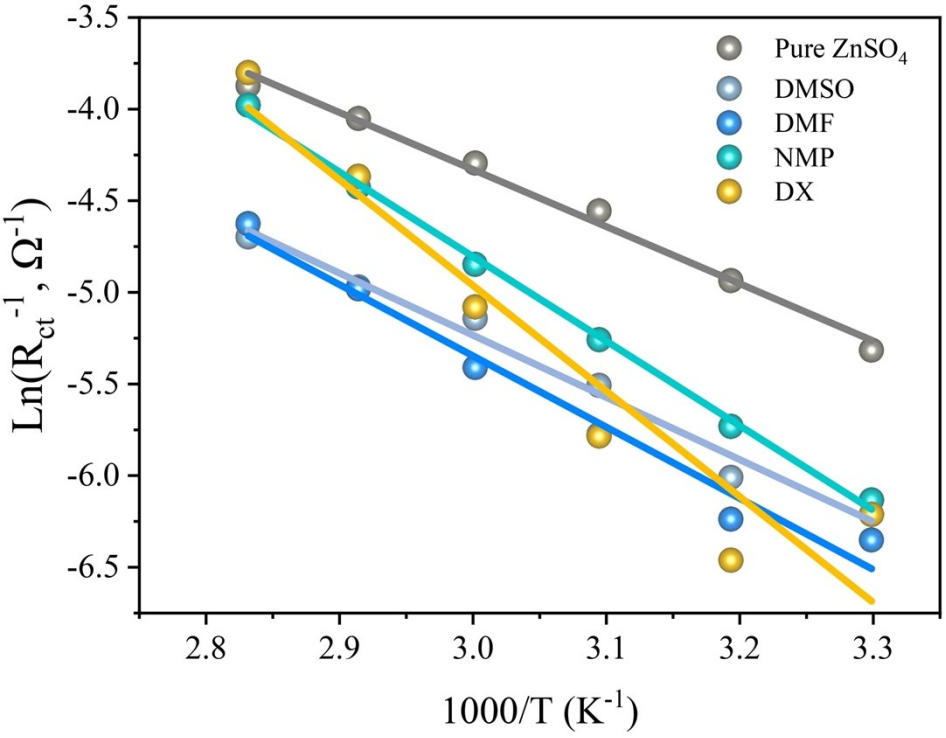

Figure S2 Fitting Arrhenius curves of symmetric cells with different organic solvents additives obtained from the Nyquist plots at different temperatures.

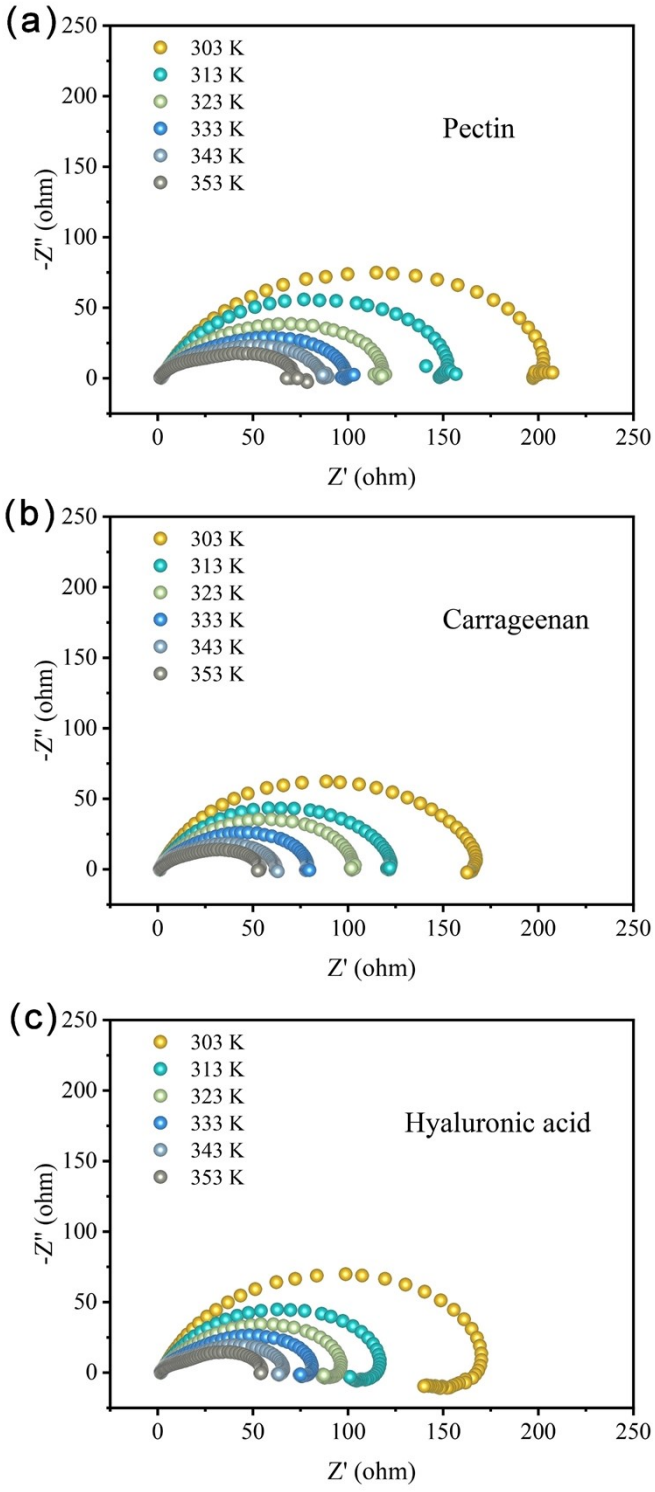

Figure S3 Nyquist plots of symmetric cells with (a) pectin, (b) carrageenan, and (c) hyaluronic acid additive at different temperatures.

Table S1 Summary of the desolvation activation energies of the symmetric cells with different electrolyte additives.

Additive	Desolvation activation energy (kJ mol^{-1})
Pectin	**17.5**
Hyaluronic acid	19.2
Carrageenan	20.2
Pure $ZnSO_4$	25.9
DMSO	28.2
DMF	32.3
NMP	38.4
DX	47.9

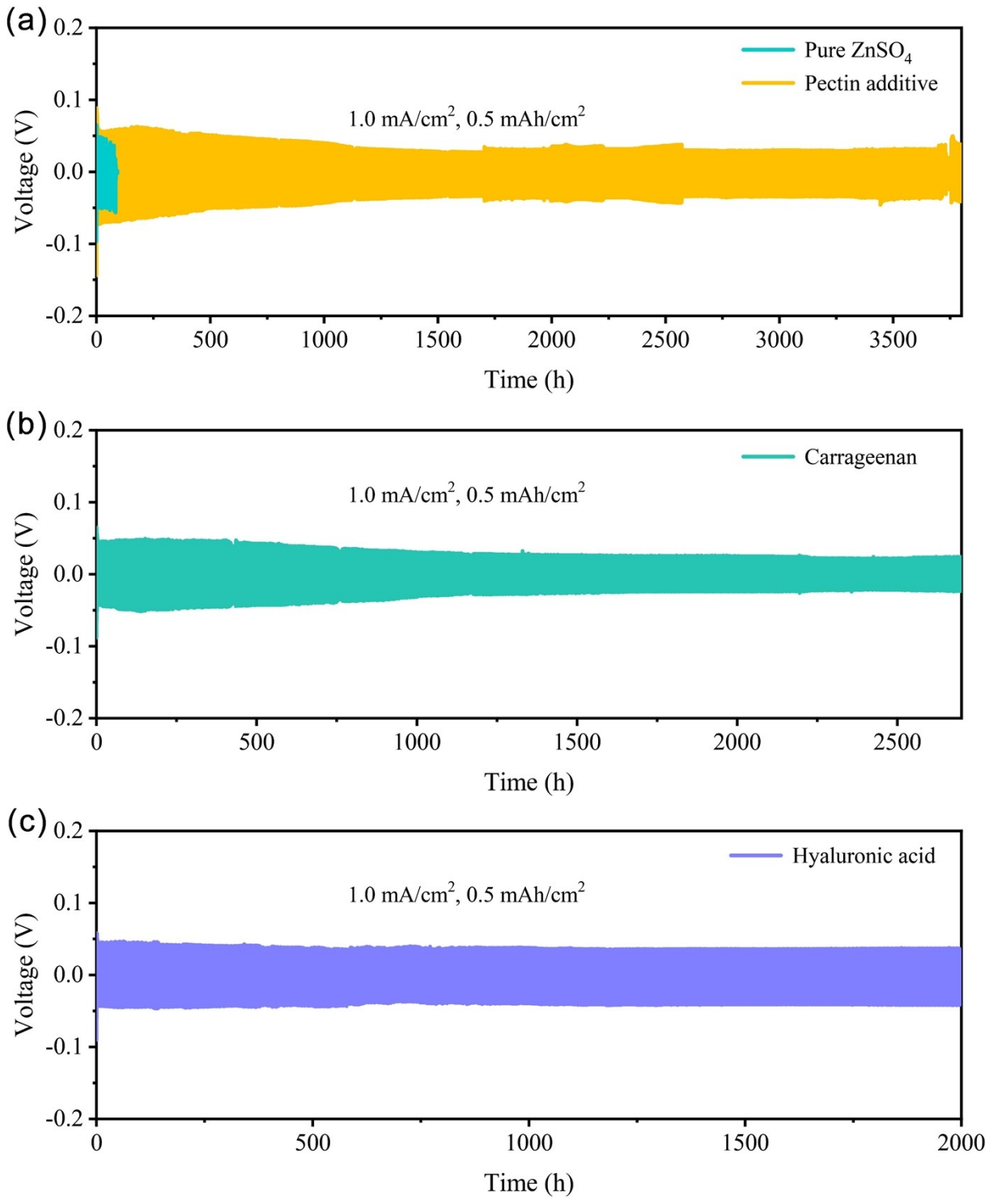

Figure S4 Cycling performance of Zn-Zn symmetric cells with (a) pectin, (b) carrageenan, and (c) hyaluronic acid additive at 1.0 mA cm^{-2} for 0.5 mAh cm^{-2}.

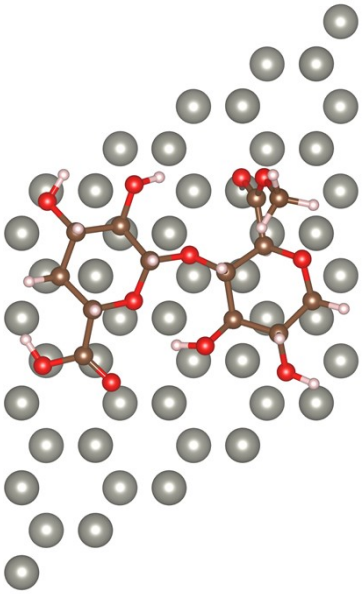

Figure S5 The top view of the adsorption configuration of the parallelly placed pectin adsorbed on Zn slab.

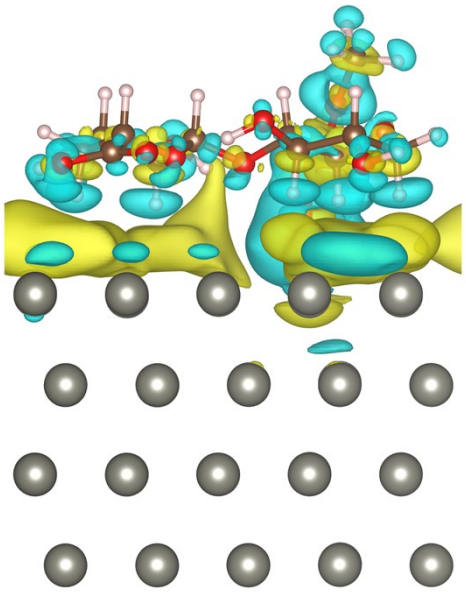

Figure S6 Charge density difference map of adsorption configuration of the parallelly placed pectin adsorbed on Zn slab.

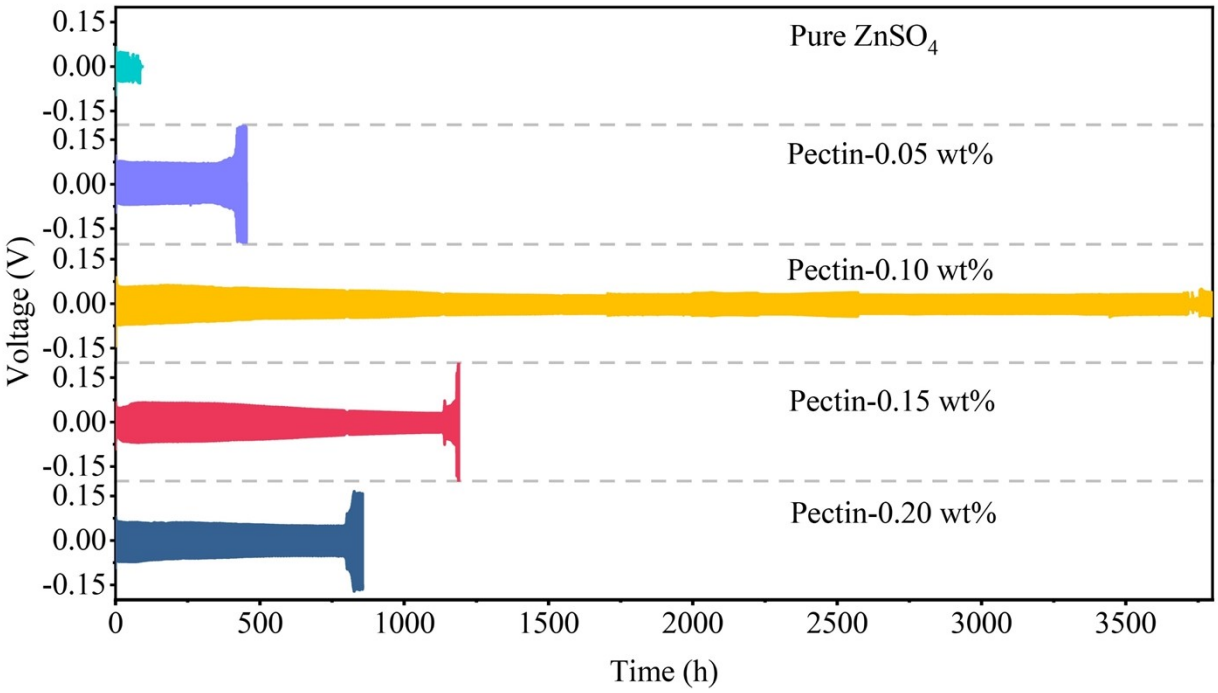

Figure S7 Cycling performance of Zn-Zn symmetric cells in different electrolytes at 1.0 mA cm^{-2} for 0.5 mAh cm^{-2}.

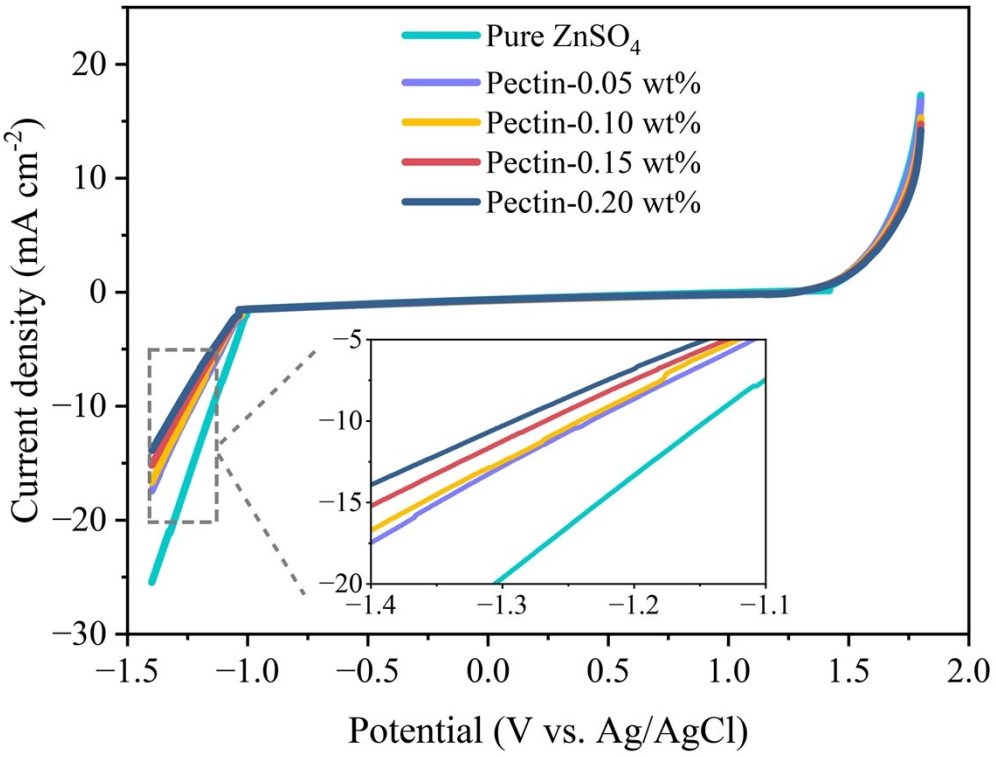

Figure S8 Electrochemical windows of the electrolytes with different pectin concentrations.

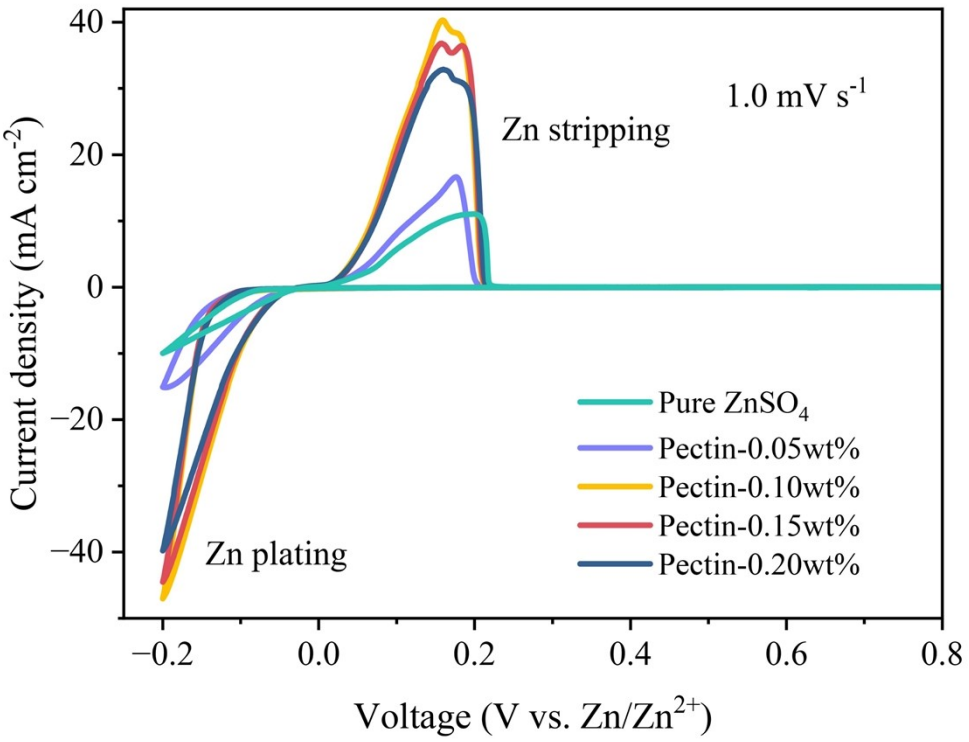

Figure S9 Cyclic voltammograms of Zn plating/stripping in $ZnSO_4$-based electrolytes with different pectin concentrations.

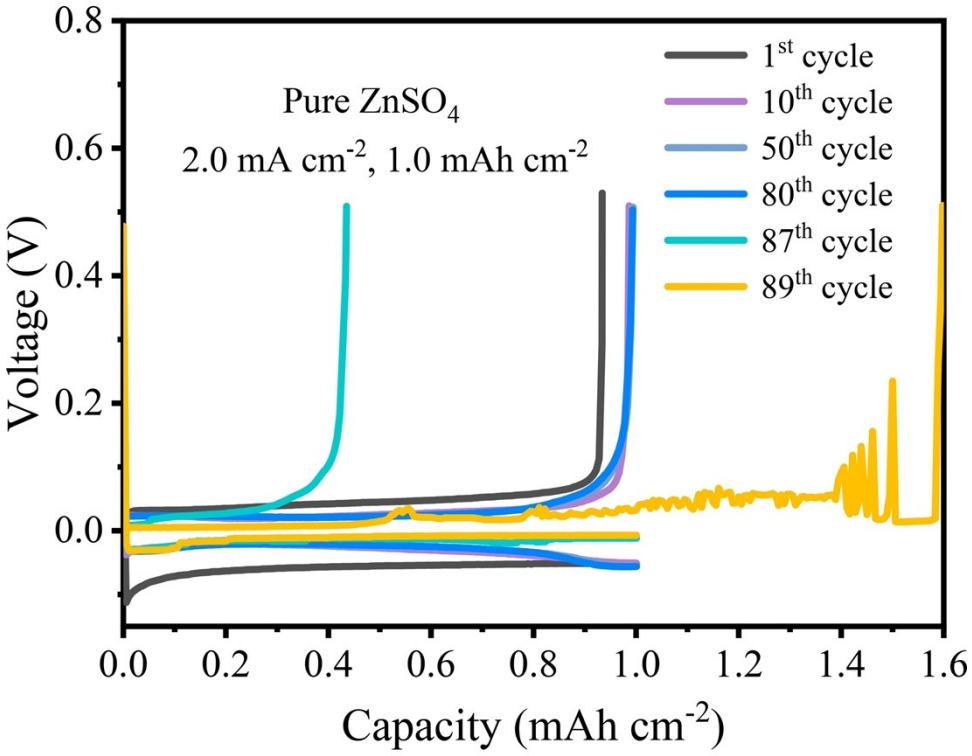

Figure S10 Voltage profiles of the Cu||Zn cells with pure $ZnSO_4$ electrolyte at 2.0 mA cm^{-2} with 1.0 mAh cm^{-2}.

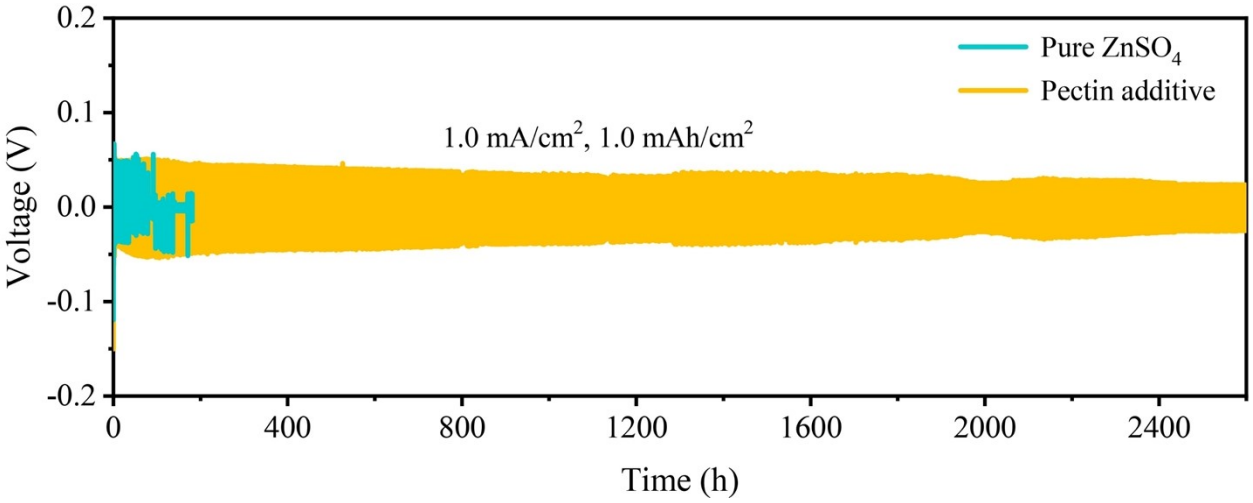

Figure S11 Cycling performance of Zn-Zn symmetric cells at 1.0 mA cm^{-2} for 1.0 mAh cm^{-2}.

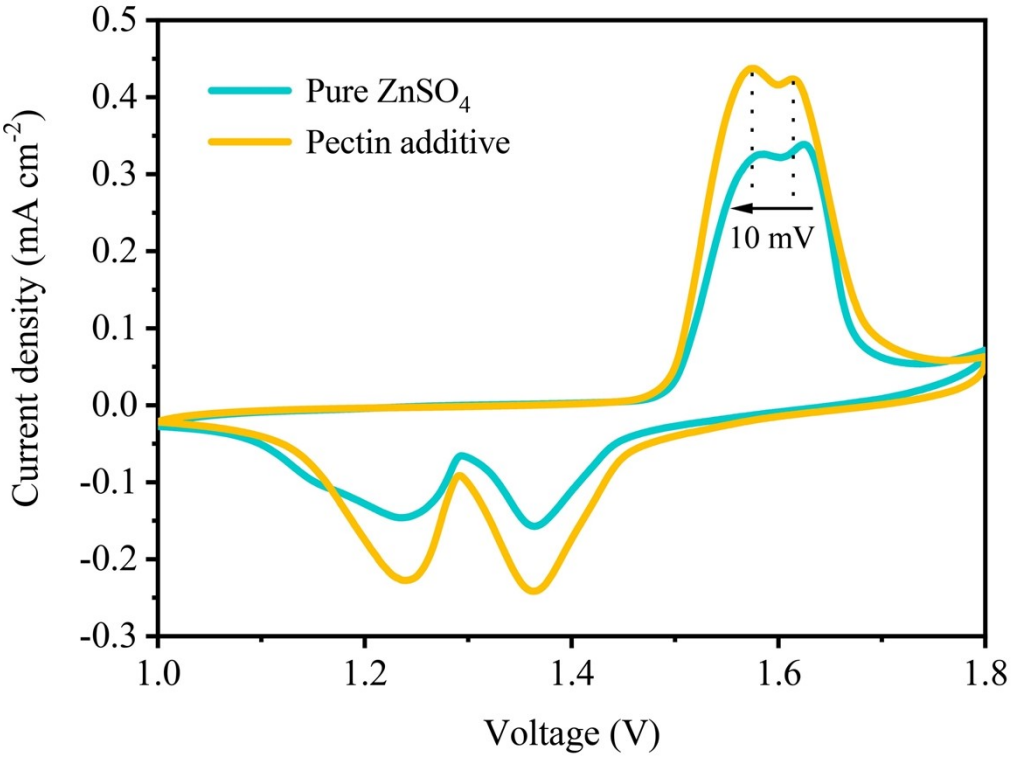

Figure S12 CV curves of the Zn||MnO_2 full cells with/without pectin additive at 0.08 mV s^{-1}.

Table S2 Summary of the performance of the symmetric cells and full cells.

Additive	Symmetric cell performance			Cathode	Full cell performance			Ref.
	Current density (mA/cm^2)	Capacity (mAh/cm^2)	Life (h)		Current density	Capacity[a] (mAh/g)	Cycle number	
Pectin	**5**	**5**	**900**	**MnO_2**	**2 C**	**175**	**500**	**This work**
	2	**2**	**2200**					
	1	**1**	**2600**					
	1	**0.5**	**3700**					
Glucose	1	1	2000	MnO_2	3.08 A/g (10C)	~112	1000	[1]
Cyclodextrin	5	5	200	V_2O_5	1 A/g	~170	200	[2]
Vanillin	1	1	1000	V_2O_5	3 A/g	249.7	500	[3]
DMAc	0.5	1	~700	MnO_2	0.5 A/g	188	880	[4]
ACN	0.5	0.5	700	PTPAn	1 A/g	~90	6000	[5]
Cysteine	5	2	350	MnO_2	0.6 A/g	96.1% retention	300	[6]
Glycerol	2	2	650	V_2O_5	2 A/g	161.2	1300	[7]
SMD	1	1	1400	MnO_2	1 A/g	~60	1300	[8]
6-AA	1	1	900	MnO_2	0.5 A/g	~100	200	[9]
Sucrose	0.5	0.5	3300	MnO_2	1 A/g	~170	800	[10]

[a]Capacity: 1 C = 308 mA/g

References

[1] Sun, P.; Ma, L.; Zhou, W.; Qiu, M.; Wang, Z.; Chao, D.; Mai, W., Simultaneous Regulation on Solvation Shell and Electrode Interface for Dendrite‐Free Zn Ion Batteries Achieved by a Low‐Cost Glucose Additive. *Angew. Chem., Int. Ed.* **2021**, 60 (33), 18247-18255.

[2] Zhao, K.; Fan, G.; Liu, J.; Liu, F.; Li, J.; Zhou, X.; Ni, Y.; Yu, M.; Zhang, Y.-M.; Su, H.; Liu, Q.; Cheng, F., Boosting the Kinetics and Stability of Zn Anodes in Aqueous Electrolytes with Supramolecular Cyclodextrin Additives. *J. Am. Chem. Soc.* **2022**, 144 (25), 11129-11137.

[3] Zhao, K.; Liu, F.; Fan, G.; Liu, J.; Yu, M.; Yan, Z.; Zhang, N.; Cheng, F., Stabilizing Zinc Electrodes with a Vanillin Additive in Mild Aqueous Electrolytes. *ACS Appl. Mater. Interfaces* **2021**, 13 (40), 47650-47658.

[4] Wu, F.; Chen, Y.; Chen, Y.; Yin, R.; Feng, Y.; Zheng, D.; Xu, X.; Shi, W.; Liu, W.; Cao, X., Achieving Highly Reversible Zinc Anodes via N, N‐Dimethylacetamide Enabled Zn‐Ion Solvation Regulation. *Small* **2022**, 18 (27), 2202363.

[5] Zhang, Z.; He, Z.; Wang, N.; Wang, F.; Du, C.; Ruan, J.; Li, Q.; Sun, D.; Fang, F.; Wang, F., Regulating the Water Molecular in the Solvation Structure for Stable Zinc Metal Batteries. *Adv. Funct. Mater.* **2023**, 33 (27), 2214648.

[6] Jiang, P.; Du, Q.; Shi, M.; Yang, W.; Liang, X., Stabilizing Zinc Anodes by a Uniform Nucleation Process with Cysteine Additive. *Small Methods* **2023**, 2300823.

[7] Yang, S.; Xue, K.; Zhang, J.; Guo, Y.; Wu, G.; Li, C.; Xia, C.; Zhang, Y.; Chen, Y.; Zhou, L., Synergistic electrostatic shielding manipulation of Na^+ and desolvation effect of Zn^{2+} enabled by glycerol for long-lifespan and dendrite-free Zn anodes. *Energy Storage Mater.* **2023**, 62, 102929.

[8] Zheng, S.; Wang, Y.; Luo, B.; Sun, L.; Duan, G.; Huang, J.; Ye, Z., In-situ formation of heterogeneous interfaces inducing surface crystallographic manipulation toward highly stable Zn anode. *Chem. Eng. J.* **2023**, 473, 145313.

[9] Huh, S.-H.; Choi, Y. J.; Kim, S. H.; Bae, J.-S.; Leea, S.-H.; Yu, S.-H., Enabling the uniform zinc deposition by zwitterion additive in aqueous zinc metal anode. *J. Mater. Chem. A* **2023**, 11

(36), 19384-19395.

[10] Zhou, L.; Yang, R.; Xu, S.; Lei, X.; Zheng, Y.; Wen, J.; Zhang, F.; Tang, Y., Maximizing Electrostatic Polarity of Non-Sacrificial Electrolyte Additives Enables Stable Zinc-Metal Anodes for Aqueous Batteries. *Angew. Chem., Int. Ed.* **2023**, 62, e202307880